1. Climate Modeling

A Model Study of a 1-D Radiative-Chemical Coupled System

Contact Person Senior Researcher, Hideharu Akiyoshi
Ozone Layer Research Team, Global Environment Group, National Institute for Environmental Studies, Environment Agency of Japan.

Keywords ozone, CO2, stratospheric aerosols, coupled processes, climate change

1. Introduction

A sudden increase in stratospheric aerosols and a gradual increase in CO2 concentration change temperature and ozone concentration in the stratosphere through the radiative processes and chemical processes, and these changes also may bring some changes in dynamical processes such as changes in propagation of stratospheric waves and global circulations, then result in a climate change. For the first step to understand the response (climate change) to an external force (e.g. CO2 increase or aerosol increase) in the complex climate system, we have constructed a 1-D (one dimensional) radiative-chemical coupled system (model). Radiative-chemical coupled processes themselves are very complex, and have quite different features at different altitudes. This study of the radiative-chemical coupled processes in a global and annual mean 1-D system will help us interpret and understand more complex dynamical-radiative-chemical processes in the real 3-D atmosphere.

We also intend to incorporate the radiative-chemical coupled processes into CCSR/NIES GCM(Center for Climate System Research / National Institute for Environmental Studies General Circulation Model), and aim to construct a dynamically, radiatively, chemically, fully coupled GCM. The chemical scheme of our coupled model is easy to combine with the GCM, doing some modifications in the spectral mean values of the absorption cross sections of the chemical constituents.

2. Basic Concept of the 1-D Coupled Model

One of the most difficult part of photochemical calculations is an accurate calculation of photolysis rates of the chemical constituents. Photolysis rates vary diurnally, seasonally, altitudinally, latitudinally, and longitudinally. Besides, it may vary seriously in the atmosphere perturbed by volcanic eruptions or CO2 increase. Generally, these photolysis rates in the normal atmosphere are tabulated as a function of zenith angles and altitudes, and people use these values (and interpolate, if necessarily) to perform their photochemical calculations. However, our idea is to perform simultaneously an multi-spectra radiative calculation which includes the scattering effects of the air molecules and aerosols, not depending on the photolysis tables. This method enable us to obtain an accurate photolysis rate self-consistently even in the perturbed atmosphere. The renewed profiles of chemical constituents in the chemical scheme are used in the radiative calculation, and renewed temperatures in the radiation scheme are also used to calculate reaction coefficients and absorption cross sections in the chemical scheme. Thus, in the radiatively chemically coupled closed system we can obtain an equilibrium profiles of temperature and chemical constituents and study their perturbations due to increased CO2 or stratospheric aerosols.

3. Outline of the 1-D Coupled Model

The stratospheric1-D radiative-chemical coupled model is useful for studying rather long-term effects of increased stratospheric aerosols and CO2 concentration on the temperature and the concentrations of the other chemical constituents from annual-mean and global-mean points of view.

* Family method is used for the photochemical calculations (Yang et al., 1991).
* 2-stream approximation method (Hybrid modified Eddington-delta function method, Meador and Weaver, 1980) is employed for the solar radiative transfer calculations (131 spectral bins).
* H2O, CO2, and O3 random models are employed for the terrestrial infrared radiative transfer (31 spectral bins).
* Vertical resolution is 2.5km of the log-P coordinates.
* Time resolution for the radiative calculation is 8 hours, while 10 minutes for the chemical calculation.
* A convective adjustment method is used in the troposphere.
* Tropospheric cloud is not considered. But, reflection of solar radiation by the clouds is included in the surface albedo of the model; it is adjusted so that the planetary albedo of the earth (the atmosphere, the cloud, and the ground surface) become 0.3. The value of the surface albedo is 0.355 for this model. No infrared effects of cloud are considered.
* Diurnal mean solar heating rates and photolysis rates are calculated by averaging them at each time of one hour interval, and it is assumed that these mean values continue all day long.

3. Results

3-a) Radiative-photochemical equilibrium profiles

Radiative-photochemical equilibrium temperature and concentrations of 41 chemical species were calculated. They are all within the realistic values in the stratosphere.

Vertical distributions of temperature, ozone,

methane, and CFCs are presented in Figures 1a, 1b, and 1c.

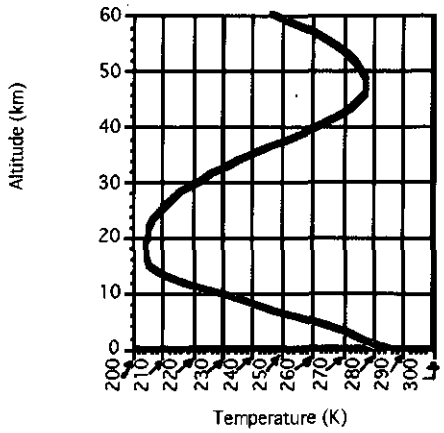

Figure 1a. Vertical distribution of radiative-chemical equilibrium temperature.

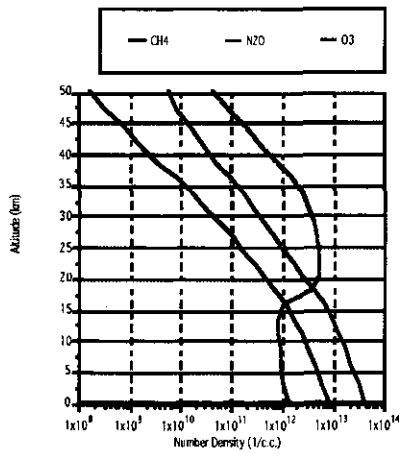

Figure 1b. Equilibrium vertical profiles of methane, nitrous oxide, and ozone.

3-b) Perturbation of the Atmosphere due to Abruptly Doubled CO2

Figure 2 shows mixing ratio variations relative to their radiative-photochemical equilibrium values at 30km, when volume mixing ratio of CO2 is suddenly doubled from 340ppmv to 680ppmv on the day number 0. Temperature falls about 6K at this altitude by one month later, then ozone is increased about 3%. Almost all photolysis rates at this altitude are decreased due to the ozone increase at and above this level. Due to the variations of both photolysis rates and chemical reaction rates, however, mixing ratios of some constituents are increased, while the others are decreased. It is noted that the mixing ratios of many chemical constituents vary with the temperature at this altitude, but some constituents have quite different time-scales of variation.

We are also planing gradual CO2 increase experiments, and volcanic aerosol increase experiments.

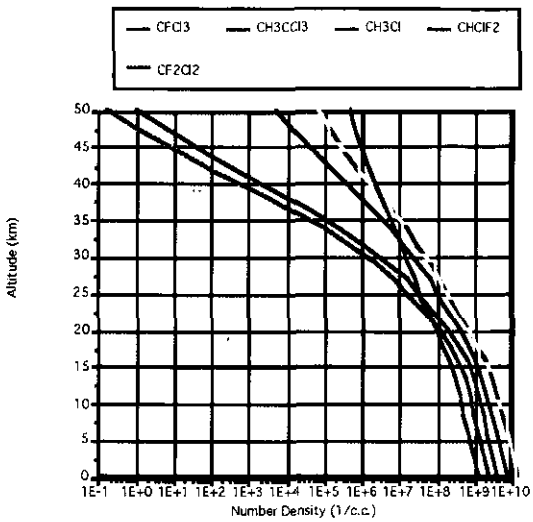

Figure 1c. Equilibrium vertical profiles of CFCs.

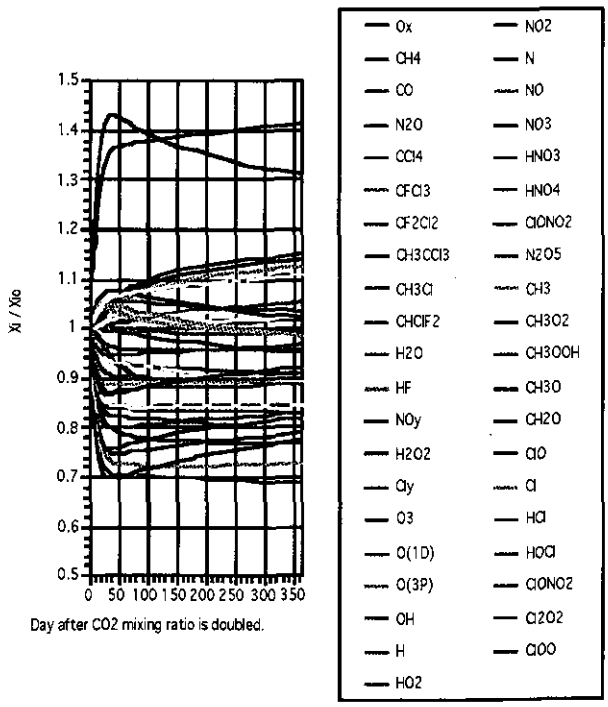

Figure 2. Variation of relative concentrations of chemical constituents to their initial values at 30km after CO2 is suddenly doubled at all altitudes.

References

Meador, W. E., and W. R. Weaver, 1980: Two-stream approximations to radiative transfer in planetary atmospheres: a unified description of existing methods and a new improvement. J.Atmos.Sci., **37**, 630-643.

Yang, H., E. Olaguer, and K. K. Tung, 1991: Simulation of the present day atmospheric ozone, odd nitrogen, chlorine and other species using a coupled 2-D model in isentropic coordinates. J. Atmos. Sci., **48**, 442-471.

Ultra-high resolution modeling of the tropical atmosphere

Contact Person Kensuke Nakajima
Center for Climate System Research, University of Tokyo
Keywords cumulus convection, tropical atmosphere, numerical modeling, air-sea interaction

1.Backgrounds

Importance of cumulus convection in the energy and hydrological cycle of the earth's atmosphere can never be over-emphasized. But its smallnesses in temporal and spatial scales compared to the scale of the global atmosphere as a whole prevent it from explicitly calculated in current generation of GCM's. Thus every GCM includes cumulus parameterization, which have many uncertainties that arise from our poor understandings on the interaction between large scale motions and the cumulus clouds.

To quantify the interaction between cumulus convection and large-scale(LS) motion, so called 'cumulus ensemble models'(CEM) had been used since early 1980's. It is a large domain (O(100km)) cloud convection model, where one imposes an 'observed' large-scale forcing and analyzes the results in a statistical manner. There remains, however, a critical defect in this CEM approach; in the real atmosphere the interaction between cumulus clouds and large-scale motion is two-way, whereas in CEM it is forced to be one-way (large-scale motion is cause and cumulus convection must be its result). This can be straightend by doing cumulus resolving GCM simulations, but computational resource requirement for such calculations is enormous (at least 1,000,000 times that is available today). Still, two-dimensional calculation is within the power of current generation vector supercomputer.

As documented in Nakajima(1994a), I constructed a two-dimensional cloud model that covers a domain of 16384km. Its high spatial resolution (2km) and incorporation of cloud microphysical processes allows cumulus convection to be represented explicitly. At the same time, the domain is as large as the longitudinal size of the pacific. Suface latent and sensible heat fluxes are supplied from the underlying fixed temperature ocean using bulk formulae. The troposphere of the model is cooled at a (basically) constant rate, crudely simulating the effect of radiation. The time marching can be continued 10days or longer with 24 hour CPU time using the SX-3 at CGER,NIES.

The construction of numerical model alone is not sufficient for examination of the cumulus-LS interaction; we must find a set-up where such interaction naturally occur. Wind induced surface heat exchange (WISHE) provides one of such mechanism as reported by Nakajima(1993), and Nakajima(1994b) reported experiments concerning wave-CISK (Conditional Instability of the Second Kind).

Although the convections were generated over the ocean, both of the above two, i.e. WISHE and wave-CISK, can be said as *internal* mechanism in the atmosphere; the sea surface temperature (SST) was fixed and horizontally uniform. In this report, the effect of underlying ocean is examined.

2. Convection over inhomogeneous SST

It is widely accepted that convective activity is strongly modulated by sea surface temperature distribution. This is true both in the climatological sense and in the deviation from it; Inter-tropical convergence zone is an example of the former and ENSO (El Nino and Southern Oscillation) is of the latter. However, precise relationship between SST and convection is still controvertial. One of the difficulties comes from ambiguity in the interaction between cumulus clouds and the large-scale environment.

Therefore, in this study, I will examine the response of the large-scale cloud organizations to underlying SST distribution. In all of the experiments that will be presented below, SST varies sinusoidally in 29 ± 1 K with horizontal wavenumber 1; it is held constant in time. The Colioris parameter is set to 0 unless noticed particularly. Time integrations are continued for $11 \sim 24$ days.

3. Results

a. Importance of surface wind speed

Fig.1 shows the convective activity in case FW, where wind speed for surface flux calculation, V_{sfc}, is fixed(3m/s). In broad sense, convection responds to SST distribution in a rather simple manner; maximum rainfall occurs around $x = 1024km$, where SST is highest. However, more closely examined, clusterings with lifetime of O(1day) and spatial scale of 500km are evident; under these scales the relationship between SST and convection has an stochastic nature.

Fig.2 shows that of case VW, where V_{sfc} is equal to the horizontal wind speed that is calculated in the simulation, so that it depends on x and t. In this case, the maximum rainfall does not occur over the highest SST region; convetive activity exhibits a secondary minimum there. Clustering of convection in the smaller scale is more evident than in case FW.

The difference between the large-scale modulations in case FW and that in case VW comes mainly from the spatial distribution of surface wind. When convection occurs in a symmetric manner with respect to the SST maximum as in both cases, time averaged horizontal wind speed is smallest at the SST peak. Then, the surface heat fluxes is smaller

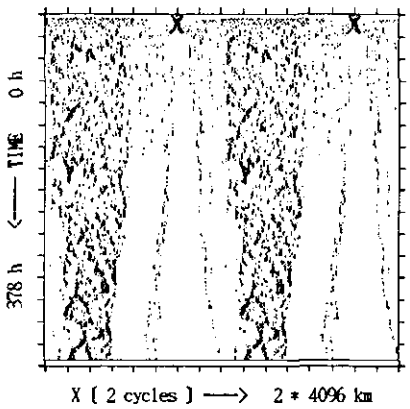

Figure 1: Time evolution of rainfall distribution in case FW. Two cycles of 4,096 km domain is shown from left to right. Time goes down from 0 h to 378 h.

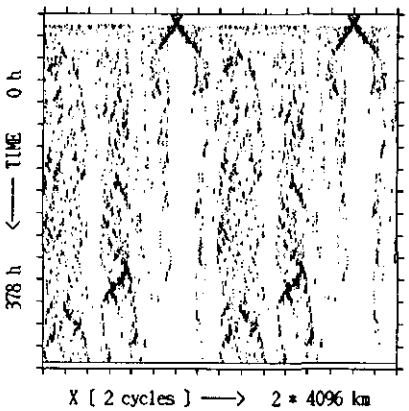

Figure 2: Time evolution of rainfall distribution in case VW. Two cycles of 4,096 km domain is shown from left to right. Time goes down from 0 h to 378 h.

there, so that moist entropy of the low level atmosphere becomes lower than the air in the regions off the peak. Clouds follows this moist entropy distribution, thus its relationship between SST becomes indirect.

b. Effect of the earth's rotation

Fig.3 shows the rainfall in case R, where the effect of the earth's rotation is included ($f = 10^{-4}$). In contrast with previous two cases, the response of convection to SST inhomogeniety is quite weak. More closely examined, stationary variation with $\sim 1000km$ wvelength is noticable; this is remnant of Ekman CISK [Charney and Eliassen, 1964].

The weak response is related to the temperture variation in the middle troposphere; it is warmer(cooler) over the higher(lower) SST region. As a result, convective instability becomes almost

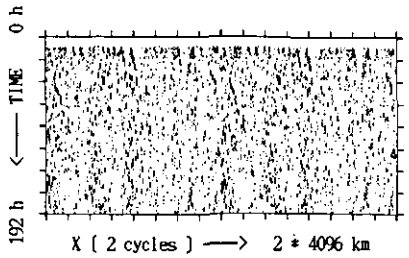

Figure 3: Time evolution of rainfall distribution in case R. Two cycles of 4,096 km domain is shown from left to right. Time goes down from 0 h to 378 h.

horizontally uniform in spite of the SST variation. It should be noted that such mid tropospheric temperature variation is maintainable only in the presence of non-zero f. Also I point that the degree of this cancellation of SST is scale dependent. In fact another experiment (not shown) where SST is varied in shorter wavelength exhibits much stronger response.

c. Wave-CISK over inhomogeneous SST

Fig. 4 shows the rainfall in case CISK, where the upper troposphere was cooled more strongly and wave-CISK is prefferable. In a broad scale, the convective activity is responding positively to SST. At the same time, convective activity propagates with phase velocity $\sim 20m/s$ in left and right. This type of propagating behavior is an exemplification of wave-CISK. The wavelength in the active region ($\sim 2000km$) is shorter than that in homogeneous SST case [see Fig.3 of Nakajima(1994b)].

In short, wave-CISK convection persists even in inhomogenous SST, and responds to SST in a time- and space-filtered manner. However, response to SST is again scale dependent. In a case where SST is varied in a wavelength shorter than the preffered wavelength of wave-CISK (not shown), the lowest SST region became a secondary *maximum* of rainfall. This results from a phase-lock effect of SST and non-lineality of wave-CISK [see Nakajima(1994a)].

d. WISHE over inhomogeneous SST

Fig.5 shows the rainfall in case WISHE, where basic wind plus model computed wind was used in surface flux calculations and WISHE is possible. Here, WISHE wave appeares as a modulation of convective activity propagating to the right. During the propagation, its strength modulates in time; it is stronger over (or slightly upwind side of) the high SST region. In other words, time-averaged convective activity is strongest over warm SST region, and occur as large-scale propagating pattern.

Compared with the homogeneous SST case [fig.1 of Nakajima(1993)], phase propagation of WISHE wave is much less regular; spatial structure is also more complex, i.e., it is no longer simple wave-number one pattern. This might be explained as a

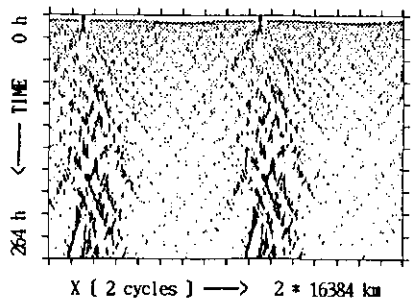

Figure 4: Time evolution of rainfall distribution in case CISK. Two cycles of 16,384 km domain is shown from left to right. Time goes down from 0 h to 264 h.

non-linear interaction between propagating WISHE wave and SST-induced stationary component.

As in the wave-CISK case, the WISHE's response to SST variation is also scale dependent. In a case where SST varies in 4000km, the response became much weaker(not shown).

4.Concluding remarks

As described above, the relationship between the spatial distributions of convective activity and SST is rather complex; it varies depending on the model parameters in particular set-up's. Therefore, careless simplification or generalization is dangerous.

Such complexity is not unique to the cumulus resolving approach. Thus, careful comparison between the results of the present approach and GCM approach is necessary; it will be helpful to determine whether a particular problem exists in the real atmosphere or originates from the deficiencies in either(or both) approach.

The SST distribution was fixed in this study; relaxing this point, i.e., coupling the cumulus resolving model with an active ocean model will be an interesting extension. In particular, observational evidence suggents that the response of the ocean to the cumulus convection occurs not only in the large-scale but also in smaller scales; the latter can be studied only by such an ultra-high resolution coupled atmosphere-ocean models.

Acknowledgements

Computations are done by SX-3 at CGER. The author very much thanks to the staff members of NIES for the technical supports.

References

1. Charney,J.G. and Eliassen,A. (1964): On the growth of the hurricane depression. J.Atmos.Sci., 21, 68-75.

2. Nakajima, K. (1993): Ultra-high resolution modeling of the tropical atmosphere. in CGER'S SUPERCOMPUTER ACTIVITY REPORT 1992.

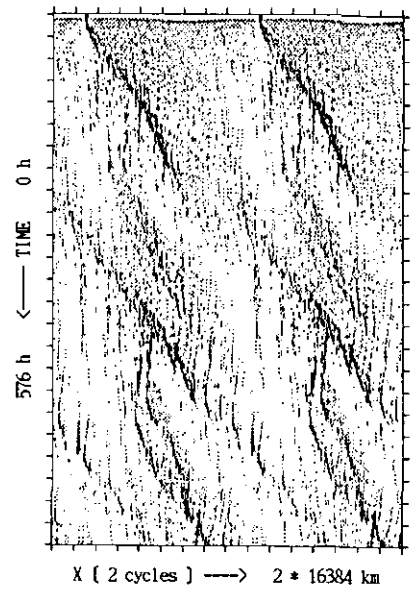

Figure 5: Time evolution of rainfall distribution in case WISHE. Two cycles of 16,384 km domain is shown from left to right. Time goes down from 0 h to 576 h.

3. Nakajima, K. (1994a): Direct simulation of large scale organizations of cumulus convection. Ph.D Thesis at University of Tokyo. (in Japanese. English version will be available from author.)

4. Nakajima, K. (1994b): Ultra-high resolution modeling of the tropical atmosphere. in CGER'S SUPERCOMPUTER ACTIVITY REPORT 1993.

Development of an Atmospheric General Circulation Model for Climate Research

Contact Person	Atusi Numaguti Atmospheric Environment Division, National Institute for Environmental Studies, Japan Environmental Agency.
Research Organization	Seiji Sugata, Shigeki Mitsumoto, Yukari N. Takayabu, Itsushi Uno National Institute for Environmental Studies Masaaki Takahashi, Teruyuki Nakajima, Masahide Kimoto, Akimasa Sumi Center for Climate System Research, University of Tokyo.

Keywords	climate model, atmosphere, parameterization, land surface, clouds, transport

1 introduction

A quantitative evaluation of climate change such as the global warming is impossible without a high-quality numerical model which describes the dynamics of the climate system and the circulations of the energy and material. The purpose of this research is to develop a numerical climate model which enables research on the mechanism of the climate change with the time scales ranging from several years to hundreds of years. We have developed an atmospheric part of the model, *i.e.*, an atmospheric general circulation model, which is named CCSR/NIES AGCM.

The basic standpoint in the development is to build the model based on sound physical basis and less dependent on empirical parameters. Effective model code was employed to make possible a long-term integration with high resolution. In addition, considerable attention was paid to the readability and module compatibility of the model code to enable community use of the model.

In order to make the model suitable for climate research, developments on the following three points are required. The first is the improvement of the parameterization of physical processes. Particularly, the parameterizations of radiative transfer, cloud process, and land-surface processes are very important. The second is the preparation of dataset for use of the model as boundary condition. The third is the testing on the model ability for reproducing the current climate and the tuning of the model parameters, the parameterization schemes, and the boundary conditions.

2 Model Description

The model is based on a simple global atmospheric model developed at University of Tokyo (Numaguti, 1993). The model uses spectral transformation method in horizontal and grid differentiation on sigma coordinate in vertical. The physical parameterization includes a sophisticated radiation scheme with two-stream k-distribution method, simplified Arakawa-Schubert cumulus scheme, prognostics of cloud water scheme, turbulence closure scheme with cloud effect, orographic gravity wave drag, and a simple land-surface model. The characteristics of the model are summarized as follows.

Basic Equations : Three-dimensional hydrostatic primitive equations on sphere with normalized pressure (σ) coordinate.

Prognostic Variables : Horizontal velocity, temperature, surface pressure, specific humidity, cloud liquid water, soil temperature, soil moisture, snow depth.

Discretization : Spectral transformation method with Gaussian grid in horizontal and an grid differentiation (Arakawa and Suarez, 1983) in vertical. Leap-frog scheme for time integration.

Resolution : Variable, standard resolution is T42 (2.8° grid) 20 levels and T21 (5.6° grid) 20 levels.

Physical Processes : Two-stream k-distribution scheme for radiative transfer
Simplified Arakawa-Schubert cumulus parameterization
Estimation of cloud liquid water by prognostics of the total water content
Mellor-Yamada level 2 turbulence scheme.
Bulk scheme for surface fluxes (Louis, 1979)
Multi-layer treatment of land-surface energy budget and hydrology
Orographic gravity-wave drag scheme (McFarlane, 1987).

3 Results

3.1 Simulated Interannual Variation with Ten-year Observed SST

An CCSR/NIES AGCM integration with ten-year observed SST (sea surface temperature) is performed and the results are compared with observed field in terms of interannual variability. The horizontal resolution is T21 (~ 600km transform grid) and with 20 vertically levels (σ = 0.01 top). This integration is based on AMIP (Atmospheric Model Intercomparison Project) international project, in which about 30 AGCM in the world are participated. It is found that overall magnitude of interannual variance in the troposphere is comparable, but somewhat smaller than, the observations. Temporal correlations between simulated and observed monthly-mean anomalies are significant (0.64 for 850hPa zonal wind) in eastern equatorial Pacific (Figure 1), but the correlation drops to insignificant values outside the tropical Pacific In particular, no significant correlation is observed in the mid-latitudes except for North American region. However, this does not necessary show the weakness of the model because it is known that the interannual behavior of the mid-latitude is as rather chaotic and the factors other than SST are important there.

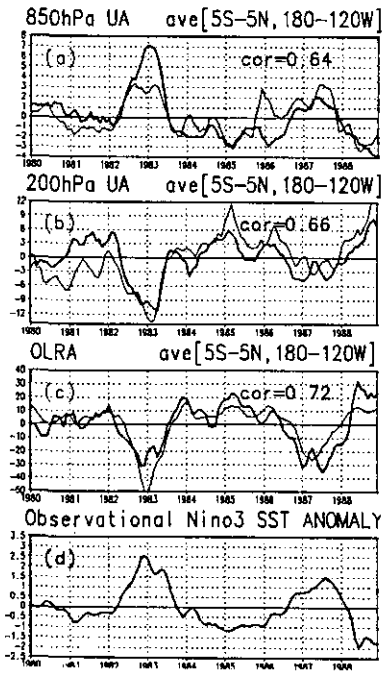

Figure 1 Time-series of anomalies averaged over 5°S-5°N, 180°-120°W for (a) 850hPa zonal wind , (b) 200hPa zonal wind , (c) OLR , (d) observational Nino-3 SST anomalies. 3-month running means are applied and thick lines for observations, thin lines for simulated results , "cor" indicates the simultaneous correlation coefficients between observations and simulations.

Figure 2 compares correlations between simulated and observed OLR (outgoing longwave radiation) fields with observed NINO3(eastern equatorial Pacific region) SST index. The response of eastern Pacific is reasonable but the signal in Indonesian region is weak and is shifted eastward. There is a moderate signal in Indian region in the model whereas the signal is very weak in the observation. It appears important to simulate accurately the spatial distributions of convective anomaly not only in the immediate neighborhood of the largest SST anomalies but also in some key regions such as the western Pacific and Indian monsoon regions. Improvements of the model in this respect is important future study.

Near-future plan in this study includes longer-time integrations up to 40 years with GISST observed SST dataset and ensemble simulation with different initial conditions.

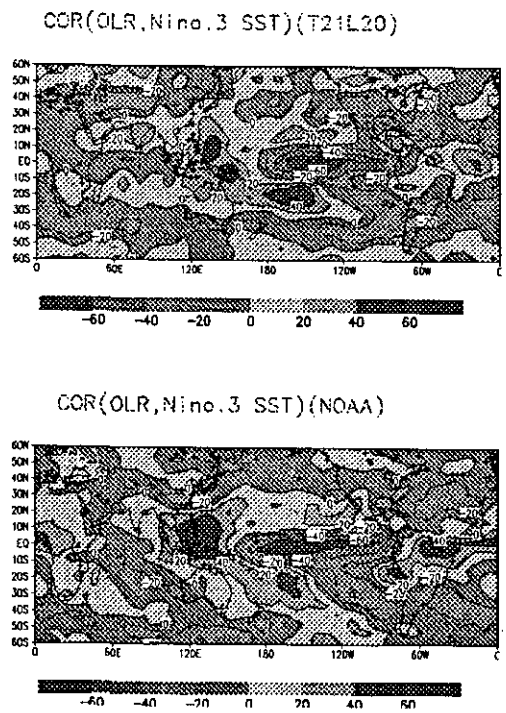

Figure 2 Mean correlation of the NINO3 (eastern equatorial Pacific) SST with OLR (a) model result, (b) observation.

3.2 Development of Atmosphere-Ocean Mixed Layer-Sea Ice Coupled Model

The CCSR/NIES AGCM is coupled with a simple thermodynamics-only slab ocean model and a sea ice model in order to study the equilibrium response to the climatic perturbation such as CO_2 doubling. The ocean in this model is represented as 50m-depth well mixed layer without motion. The effect of ocean circulation is taken into consideration by specifying heat flux distribution at the bottom of the layer. The sea ice

model is also a simple thermodynamic model without motion. Thus the prognostic variables in the oceanic part are the temperature of the ocean layer and the sea ice thickness.

A series of preliminary integration is performed to make a suitable heat flux distribution at the bottom of the layer. We are planning integrations of this simple coupled model concerning the global warming issue including the effect of increasing CO_2, other trace gases and the aerosols.

3.3 *Role of Runoff Processes in Atmosphere-Land Water Circulation*

The sensitivity of global water cycle to the treatment of runoff is examined through experiments by CCSR/NIES AGCM. The surface hydrology model used is a single reservoir model like the bucket model, but runoff was made to occur even in unsaturated conditions. Two distinct types of runoff processes are considered. One is the surface runoff, which represents the flow of water on the saturated soil into streams directly. The second is the drainage runoff, which represents the gravitational drainage of soil water below rooting depth. They are simply formulated as follows:

$$R_S = F_I \cdot (W/W_S)\,, \qquad (1)$$

$$R_D = R_{D0} \cdot (W/W_S)^n\,, \qquad (2)$$

where R_S is the surface runoff rate, R_D is the drainage runoff rate, W is the soil wetness, W_S is the saturated soil wetness, F_I is the rate of water input (sum of the liquid precipitation and snowmelt), and R_{D0} is the saturated drainage runoff rate. n is a parameter greater than one. The evaporation rate E is represented by

$$E = f(W) \cdot E_P\,, \qquad (3)$$

where E_P is the potential evaporation rate, and $f(W)$ is the water stress factor. E_P is determined by the surface heat balance with the assumption of no water stress, and,

$$f(W) = \min\{W/W_C, 1\}\,, \qquad (4)$$

where W_C is the critical soil wetness.

The boundary conditions are idealized for simplicity. Meridionally uniform two flat continents and two oceans are placed alternately and zonally uniform sea surface temperature is prescribed with an idealized seasonal variation.

The following three experiments are performed.

1. **SFC** : an AGCM experiment with the surface runoff scheme
2. **DRN** : an AGCM experiment with the drainage runoff scheme
3. **S_D** : calculation of the surface water balance with the surface runoff scheme using F_I and E_P of the experiment DRN as input.

The difference between S_D and DRN represents the direct effect of altering runoff treatments without the indirect effect through the change of F_I and E_P. The parameters in (2) are tuned for SFC and DRN to give almost the same soil wetness on the global and annual average.

The most significant direct effect of altering runoff schemes from the drainage runoff to the surface runoff is the suppression of runoff during the snowmelt season in the high latitudes (Fig. 3). Hereafter, our analysis is focused on the variables averaged over the land in high latitudes, 55° to 72°. The seasonal cycle of the water budget in this region for DRN case is shown in Fig. 4 and the differences of hydrological variables between the experiments are shown in Fig. 5. The direct effect of altering runoff schemes (broken lines) indicate that the suppression of runoff during the snowmelt season was followed by significant increase of soil wetness and evaporation. The total differences including feedback (solid lines) indicate, however, a smaller increase of evaporation with the decreased potential evaporation. The decrease of potential evaporation was mainly due to surface cooling by the increased evaporation. The radiative effect was not significant. The rain (liquid precipitation) was also enhanced during the same period. Persistence of the soil wetness is strengthen by these indirect effects with the enhancement of rain and the suppression of potential evaporation.

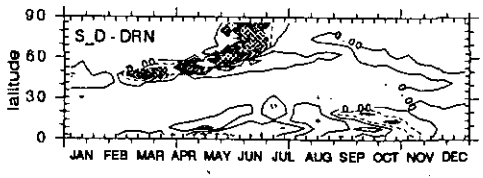

Figure 3 Difference of the calculated runoff (S_D - DRN). Latitude-time cross section of the zonal mean over land. Values less than -10 mm/month are densely hatched.

Water balance at the land surface is governed by the following equation:

$$\frac{dW}{dt} = F_I - E - R\,. \qquad (5)$$

If F_I and E_P are given constant and R is specified as a function of W and F_I as in (1) or (2), the equilibrium soil wetness, W_E, can be calculated by putting the left hand side of (5) to zero, together with (3) and (4). W_E is plotted as functions of F_I and E_P in Fig. 6(a) and (b) for $R = R_S$ and R_D, respectively. Considering the change of F_I and E_P with E (indirect effects), the

equation for δW, the perturbation of W from W_E, can be derived with linear approximations:

$$\frac{d\delta W}{dt} = -\left[E_P \frac{df}{dW}\left(1 - f\frac{\partial E_P}{\partial E}\right)^{-1} \times \left(1 - \left(1 - \frac{\partial R}{\partial F_I}\right)\frac{\partial F_I}{\partial E}\right) + \frac{\partial R}{\partial W}\right]\delta W \,. \quad (6)$$

The relaxation time scale T_E can be defined by the reciprocal of the content in the square brackets. T_E is plotted in Fig. 6(c) and (d) for $R = R_S$ and R_D, respectively. Here we take $\frac{\partial F_I}{\partial E} = 1$ and $\frac{\partial E_P}{\partial E} = -2$ from the results of the experiments. Higher W_E and longer T_E for R_S case can be seen in the region of large F_I and small E_P (lower right region in each figure). This region corresponds to the snowmelt season in the high latitudes. As seen in Fig. 7, simulated W seems to follow its equilibrium value W_E with a certain lag. The characteristics of runoff process affect both the equilibrium value and the lag.

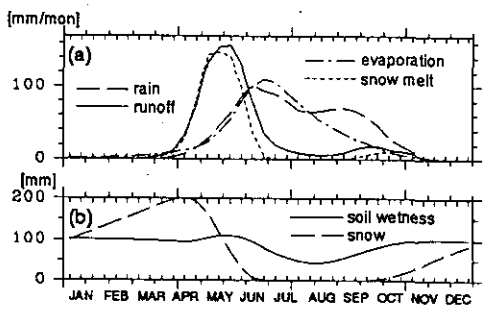

Figure 4 Seasonal cycle of the calculated water budget for DRN.

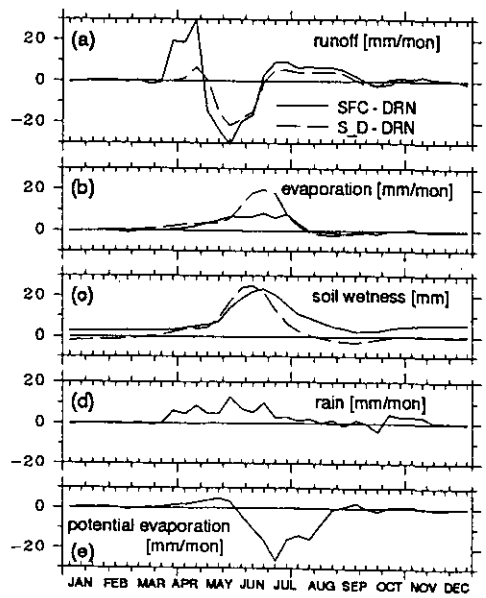

Figure 5 Seasonal cycles of the differences of hydrological variables. (solid : SFC - DRN, broken : S_D - DRN)

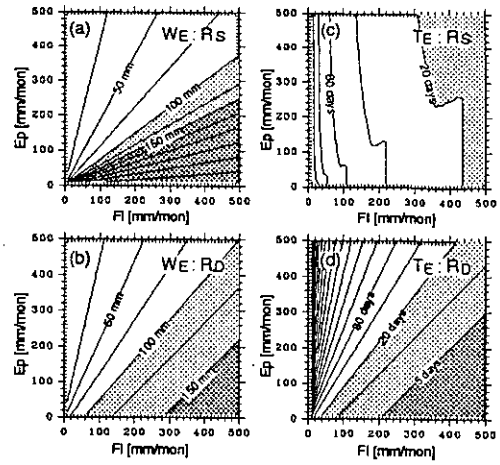

Figure 6 Equilibrium soil wetness (a),(b) and relaxation time scale (c),(d).

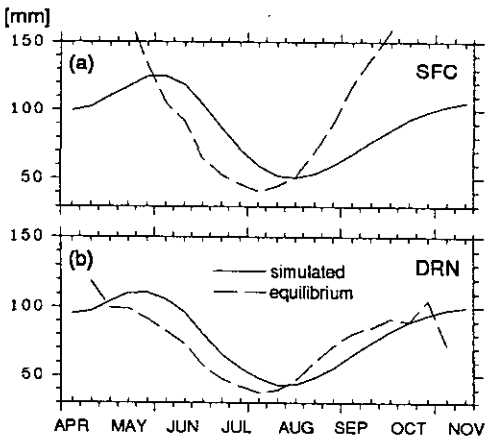

Figure 7 Seasonal variations of the simulated and equilibrium soil wetness.

3.4 Impact of cumulus convection upon global tracer transport

Cumulus convection has much influence on the global atmospheric transport since tracers are vertically diffused much by the convection. Influence of the cumulus convection upon the distribution of tracers was investigated to make fundamental basis for improvement of the transport scheme in CCSR/NIES AGCM.

Off-line transport model in the use of stored data of wind and cumulus convection obtained by integrations of the AGCM is developed. Parcels are advected by the wind except that some of the parcels in a grid with cumulus convection are lifted from the level below cloud base to that above cloud top during one integration step. Probability of lifts of particles is according to cumulus mass flux. The cumulus mass flux, the cloud base level, the cloud top level, and some other values used for the convective transport were stored at 2 hours interval and the wind data used for the

advective transport were stored at 4 hours interval. One time step of the transport model is 1 hour.

A total of 58,320 air parcels are initially released at one level near the surface (at $\sigma = 0.95$) in the northern mid-latitude with 0.5° (in longitude) and 0.5° (in latitude) intervals. Trajectories of them are calculated for one year in two different ways: one is in the model including both advective and convective transports (hereafter on-cumulus), and the other is in the model neglecting convective transport (off-cumulus). Subsidence which balances with cumulus updraft is considered in the former.

Result of the integration which starts on July 1st is shown. Figure 8(a) shows vertical distributions of the number of particles every 1km layer at each latitude band at end of first month. Off-cumulus shows about twice the number of particles in the lowest 1km layer of on-cumulus, which shows that more particles remain near the earth surface in off-cumulus than in on-cumulus owing to smaller vertical diffusion in off-cumulus. Large difference is not shown in the low-latitude, since the intrusion of particles into low-latitude from mid-latitude is mainly occurred in lower levels in both cases and vertical diffusion is sufficiently large in the low-latitude in both cases.

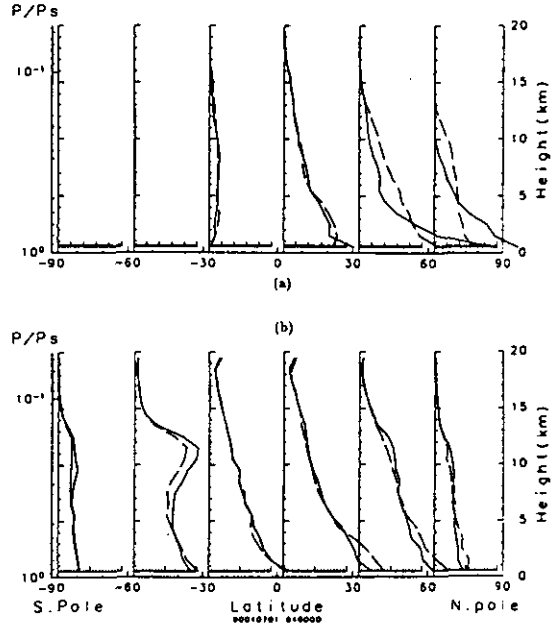

Figure 8 Vertical distributions of the number of particles at each 30° in latitude. Solid line is off-cumulus and broken line is on-cumulus. End of first month (a) and End of a year (b).

Particles disperse throughout troposphere about half year after in both cases. The difference of the vertical distribution of particles at northern mid-latitude decreases with time. At end of 12th month (Figure 8b), no distinct difference of the distributions is shown between the cases in all latitude-bands. Particle numbers decrease exponentially with height, which means that particles disperse sufficiently throughout troposphere and lower stratosphere, in all latitudes except for southern mid-latitude. Convergence around 11km height in this latitude occurs above sub-tropical jet and particles which may take much time to intrude from stratosphere to troposphere converge there.

Vertical distributions of particles at each longitude-band are also investigated in both cases (not shown). The difference between the cases is not negligible, which means convective transport by cumulus brings particles into different longitudinal distribution from non-cumulus.

4 Summary

An atmospheric general circulation model (AGCM) for use of the climate study is developed and tested in some different ways. A ten-year integration with observed SST (sea surface temperature) shows the good reproducibility of observed climate. An atmosphere–ocean mixed layer-sea ice coupled model was developed and a series of preliminary integration is performed. Sensitivity studies on land-surface processes and tracer transport are done with the model.

5 Acknowledgments

This research is supported by Global Environment Research Program of Japan Environmental Agency. Assistance by Dr. A. Abe-Ouchi, Dr. X.S. Shen, Dr. T. Oki, K. Takata, S. Emori, T. Nishimura and Y. Tsushima is greatly appreciated.

References

1. A. Numaguti, *J. Atmos. Sci.*, **50**, 1874–1877 (1993)
2. A. Arakawa A. and M.J. Suarez, *Mon. Weather Rev.*, **111**, 34–45 (1983)
3. J. Louis, *Bound. Layer Meteor.*, **17**, 187–202 (1979)
4. N.A. McFarlane, *J. Atmos. Sci.*, **44**, 1775-1800 (1987)
5. A. Numaguti, M. Kimoto, T. Nakajima, M. Takahashi, and A. Sumi, *Proceeding of AMIP Conference, Monterey, California, May* (1995).

On the Interaction Between the Circulations in the Lower- and Mid-latitudes : Meridional Distributions of (PV, θ) in the Two- and Three-dimensional Models

Contact Person Masaki Satoh
Department of Mechanical Engineering, Saitama Institute of Technology
Okabe, Saitama, 369-02, Japan

Keywords baroclinic equilibrium, potential vorticity, tropopause

1. Introduction

By using two-dimensional (2D) and three dimensional (3D) versions of the general circulation model (GCM), interactions between the circulations in the lower- and mid-latitudes are investigated. As is well known, dynamics of the mid-latitude circulation (baroclinic instability), are described by the potential vorticity (PV). Recently, Sun and Lindzen[1] tried to obtain the equilibrium states of the mid-latitudes on the assumption that PV is homogenized in the isentropic surface by baroclinic adjustment. On the other hand, in the lower-latitudes, Held and Hou[2] argued that the Hadley circulation will also homogenize PV in the isentropic surface, if the angular momentum is conserved along the stream line by using the two-dimensional model. Although it is plausible that PV tends to be uniform in the isentropic surface in the respective latitudes, it is not clear how the distributions of PV are related between both latitudes. These will be made clear by the comparison of results of 2D and 3D models [3].

2. Model

Numerical calculations are done by using CCSR/NIES GCM [4] with the resolution of T42 and 16 layers. An aqua planet model with a symmetric boundary condition (surface temperature : 300K $-$ 40 K $\times \sin^2\varphi$; φ is the latitude) is utilized. Dependencies on the rotational rates Ω will be mainly shown: $\Omega/\Omega_0 = 1/3$, 1 and 3 (Ω_0 is the rotational rate of the earth).

3. Results

Potential vorticity is defined by

$$\mathrm{PV} = -g\zeta_{a\theta}\frac{\partial\theta}{\partial p}, \qquad (1)$$

where θ is potential temperature and $\zeta_{a\theta}$ is the vertical component of the isentropic absolute vorticity, that is, the vorticity with horizontal derivatives evaluated on isentropic surfaces [5,6]. In 2D, it is expressed by

$$\begin{aligned}\zeta_{a\theta} &= 2\Omega\sin\varphi + \frac{1}{a\cos\varphi}\left(\frac{\partial u\cos\varphi}{\partial\varphi}\right)_\theta \\ &= \frac{1}{a^2\cos\varphi}\left(\frac{\partial l}{\partial\varphi}\right)_\theta, \qquad (2)\end{aligned}$$

where $l = ua\cos\varphi + \Omega a^2\cos^2\varphi$ is the angular momentum.

The meridional distributions of PV and θ are shown by the figures. In 2D (Figs. (a)–(c)), θ is horizontally uniform in the Hadley region, and is vertically uniform in the troposphere of the mid-latitudes. PV is almost zero in both regions, since the angular momentum is conserved in the Hadley region, and stratification is neutral in the troposphere of the mid-latitudes. Between both regions near the polar boundary of the Hadley cell, PV has a large gradient and the contours of PV are almost parallel to the contours of θ. The distribution of θ clearly shows the tropopause level, which exists near the contour of PV = 1.0 PVU $\times\Omega_0/\Omega$. The tropopause level in the low-latitudes is determined by the moist radiative-convective equilibrium in the whole region of the Hadley cell, and the level in the mid-latitudes is determined by the local radiative-convective equilibrium in each latitude [7].

Figs. (d)–(f) show (PV, θ) for 3D. Although the distributions of PV and θ in the Hadley cell are similar to 2D, the gradient of PV near the cell boundary is reduced. In the mid-latitudes, the contours of θ decline and cross the ground, and PV has a non-zero value as a result of the stable stratification. In the extratropic troposphere, these figures do not support the view by Sun and Lindzen [1], in which PV is homogenized along isentropic surfaces. As shown by the contour of

PV = 1.0 PVU $\times\Omega_0/\Omega$, the tropopause level does not change in the Hadley region, while it becomes higher by 100hPa than that for 2D in the mid-latitudes except for the case $\Omega/\Omega_0 = 3$. The tropopause level for 3D may be affected by baroclinic instability [8]. Although the dependency on the rotation rate is not well understood, the tropopause level at the pole seems to change in accordance with the meridional scales of baroclinic waves.

4. Summary

Comparison of the results of 2D and 3D models shows that PV distributions in the Hadley region are almost similar. In the mid-latitudes, a strong gradient of PV near the polar boundary of the Hadley cell in 2D is reduced in 3D, and the tropopause height of 3D is higher than that of 2D. Through further parametric studies of GCM, baroclinic equilibration in the mid-latitudes can be related with external parameters: e.g. rotation rates, surface temperature gradient, radiative properties, etc.

References

1. D.-Z. Sun and R.S. Lindzen, *J. Atmos. Sci.*, **51**, 751-772 (1994)
2. I.M. Held and A.Y. Hou, *J. Atmos. Sci.*, **37**, 515-533 (1980).
3. M.Satoh, M.Shiobara and M.Takahashi, *Tellus*, **47A**, in press (1995)
4. A. Numaguti, *J. Atmos. Sci.*, **50**, 1874-1887 (1993)
5. B.J. Hoskins, M.E. McIntyre and A.W. Robertson, *Q. J. R. Meteorol. Soc.*, **111**, 877-946 (1985)
6. B.J. Hoskins, *Tellus*, **43AB**, 27-35 (1991)
7. M.Satoh, *J.Atmos. Sci.*, **51**, 1947-1968 (1994)
8. R.S.Lindzen, *J. Atmos. Sci.*, **50**, 1148-1151 (1993)

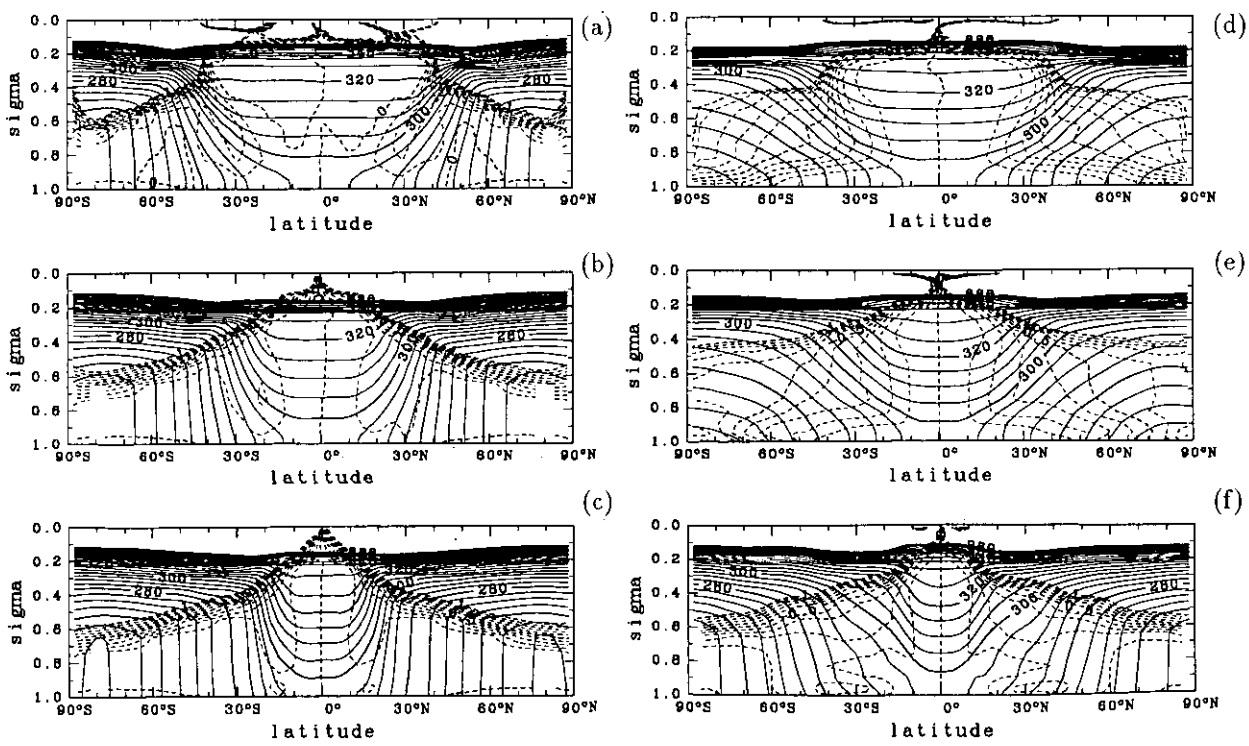

Fig.1 Meridional distributions of (PV, θ) for (a) 2D, $\Omega/\Omega_0 = 1/3$, (b) 2D, $\Omega/\Omega_0 = 1$, (c) 2D, $\Omega/\Omega_0 = 3$, (d) 3D, $\Omega/\Omega_0 = 1/3$, (e) 3D, $\Omega/\Omega_0 = 1$, and (f) 3D, $\Omega/\Omega_0 = 3$. Solid lines are θ (potential temperature) and dashed lines are PV (potential vorticity). Contours for θ range up to 380K with intervals of 5K. Contours for PV range from -1.0 to $+1.0$ PVU $\times\Omega_0/\Omega$ with intervals of 0.1 PVU $\times\Omega_0/\Omega$ (PVU = 10^{-6}m^2 K s^{-1} kg^{-1}).

Mass circulation variations due to seasonal and longer term variations in the middle atmosphere circulation

Contact Person — Senior Researcher, Kiyotaka Shibata
Second Research Laboratory, Climate Research Department,
Meteorological Research Institute, Meteorological Agency, Japan.

(Research Organization) — Masaru Chiba
Koji Yamazaki

Keywords — Middle Atmosphere, Seasonal Variations, Mass Circulation, Numerical Simulation

1. Background

Air mass flows into the middle atmosphere from the troposphere in low-latitudes, and counter outflow occurs in mid- and high-latitudes. This indicates that the middle atmosphere plays an important role in the global circulation of trace gases such as ozone, ozone depleting chemicals, carbon dioxide. The detail of this circulation, however, is still not well understood partly because of the scantness of observations. Then model simulations are expected to be a reliable tool, as a complement of observations, to investigate the global mass circulation.

2. Objective

This study is to explore the role of middle atmosphere on the global mass circulation by making and using general circulation models, which can well reproduce the characteristics of the middle atmosphere. Prior to the mass transport experiment to be made in the second year, preliminary calculations are made to investigate the effect of model resolutions on the simulated middle atmosphere. After the analysis of this experiment, a long term integration is to be made to prepare the wind data for off-line calculation of tracer transport experiment.

3. Experiment

A control experiment is made with global circulation model (GCM), which is a spectral transform model, extending from the surface to the middle mesosphere, rhomboidally truncated at wave number 13 with 23 layers (R13L23), whose resolution is approximately 8°(longitude)×5°(latitude) in the horizontal and 2.8 km in the vertical. Experiment runs are made with increased horizontal or vertical resolution models, R13L92 and R24L92. L92 models have quadruple layers, 92 layers, of about 0.7 km thickness in the vertical, while R24 model has about 5° × 3° in the horizontal. The physical processes are nearly the same as in previous version of R13L23(Shibata and Chiba, 1990).

4. Results

In both simulations with R13L92 and R24L92, westerly winds appear in the equatorial stratosphere after about two months integration, and persist with weak annual variations, whereas R13L23 does not yield westerly winds. Analysis of equatorial waves shows that Kelvin waves of about 10 km wavelength can propagate upward due to the increase in vertical resolution(Fig.1), and that the dissipation of Kelvin waves yield westerly winds.

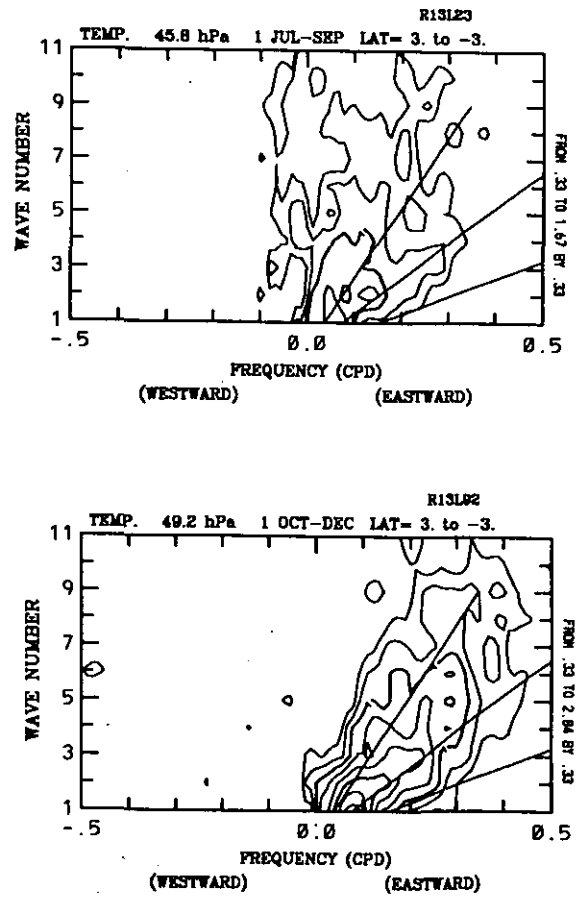

Figure 1. Power spectrum of temperature wave for R13L23(upper) and R13L92(lower).

The vertical extent of westerly winds in the persistent state is narrower in R24L92 than in R13L92, and their top heights are about 30 hPa and 10 hPa, respectively. The mixed Rossby-gravity wave is responsible for this difference. The power spectrum of meridional wind of 5-day period and wave number 4 in the stratosphere is much smaller in R13L92 than in R24L92(Fig.2). Since this wave is anti-symmetric with respect to the equator, R13 horizontal resolution is too coarse to simulate this wave. R24 is still coarse(Fig.3).

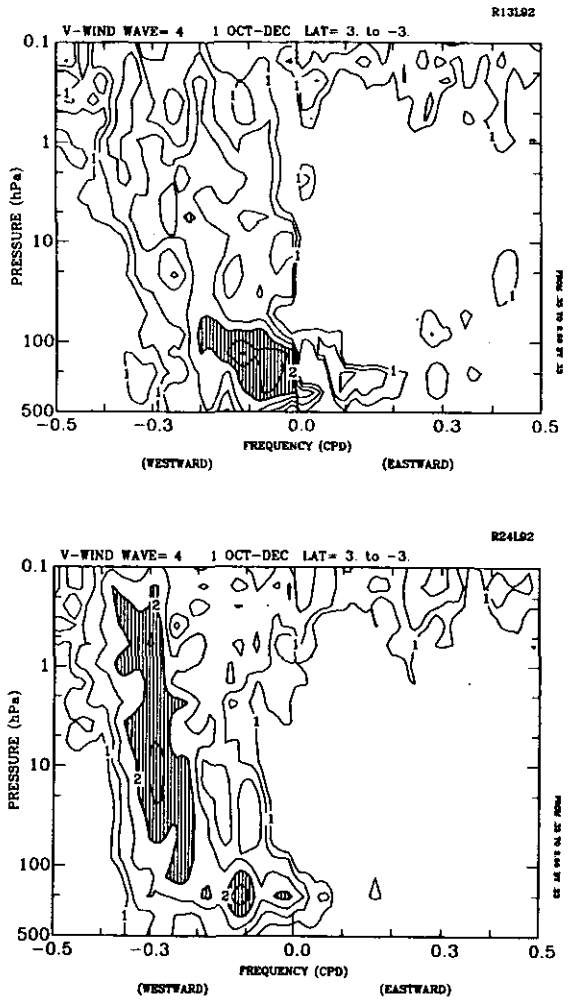

Figure 2. Power spectrum of meridional wave for R13L92(upper) and R24L92(lower).

The power of the equatorial waves in models depends on both the condition of propagation (*i.e.*, model resolution) and the strength of their source in the troposphere. To evaluate the latter effect, Hadley circulation is investigated. Mass stream function in the northern winter weakens with resolution in the tropical upper troposphere. Precipitation also decreases with resolution in the tropics(Fig.4), indicating that Hadley circulation is, at least, not intensified.

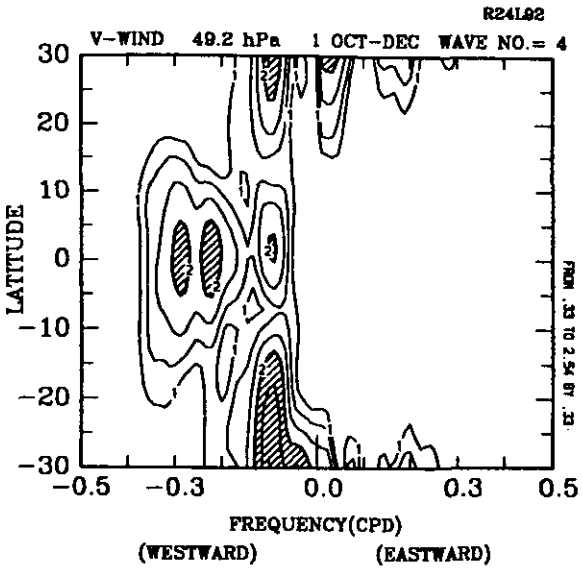

Figure 3. Latitudinal distribution of power spectrum of meridional wave for R24L92.

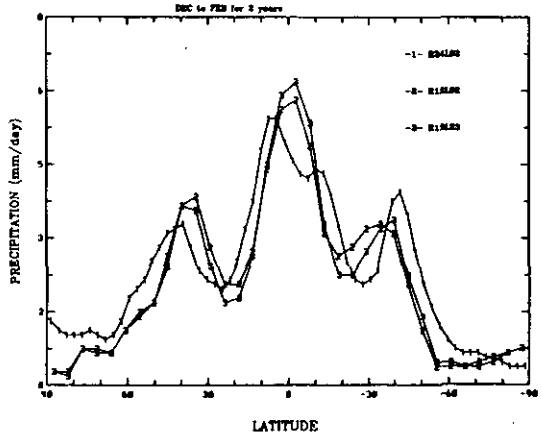

Figure 4. Latitudinal distribution of precipitation.

References

1. K. Shibata and M. Chiba, J. Meteorol. Soc. Japan, **68**, 687(1990)

The Study of Seasonal Variation of Ozone by a General Circulation Model

Contact Person Isamu Yagai,
Meteorological College
7 Asahi-cho, Kashiwa-shi, Chiba-ken, 277
(Research Organization) Shigeru Fujita, Meteorological College

Key Words ozone, seasonal variation, photochemistry, general circulation model

1. Introduction

In June 1994, a NATO workshop on atmospheric ozone as a climate gas was held in Norway and attended by 48 participants from 15 countries including the author. The objectives of this workshop were:

- to document current knowledge about ozone in the atmosphere and its impact on climate;
- to discuss the scientific issues concerning the chemical and climate aspects of ozone; and
- to identify the research needed for developing coupled chemistry-climate general circulation models.

The workshop was divided into four working groups relating to: upper tropospheric/lower stratospheric climatology; chemical modeling; climate modeling; and coupled chemistry/climate models.

In the aspects of ozone simulation by three dimensional atmospheric General Circulation Models (GCMs), it is pointed that the long term effects of the greenhouse warming may have an effect on lower stratospheric ozone through the already observed intensification of the polar winter vortex in the Northern Hemisphere. There is a possible feedback loop linking polar cooling and ozone depletion. So far the on going cooling/depletion is interrupted regularly by the redistribution of stratospheric circulation in the annual cycle. It is uncertain, however, whether a part of the effect of the ozone destruction survives the annual cycle in a way that could increase the ozone depletion in the following year.

2. Research Objective

It is also pointed out in the workshop that the certain features of the stratospheric circulations are particularly critical for modeling ozone-climate interactions. Because of the temperature dependence of certain heterogeneous reactions, it is important to get reasonable temperature distributions from GCMs. However, the large errors present in GCM simulations in winter polar lower stratosphere, which are thought to exist of insufficient wave driving by unresolved gravity waves.

The 15-layer general circulation model of the Meteorological Research Institute (MRI GCM) has still westerly biases in the northern hemisphere wintertime flow, though it has been largely eliminated by incorporating gravity wave drag parameterization due to orography. Therefore it is not suite to calculate complex heterogeneous reactions in the current MRI GCM, and we use a simplified photochemical model to see the fundamental seasonal variation of ozone, which includes Chapman reactions and the $NO-NO_2$ catalytic cycle in the stratosphere above 100 hPa.

3. Results

The model used here is the 15 layer MRI GCM which has seven layers in the stratosphere and the model top is 1 hPa. The model started from the observed atmospheric condition at 00Z 1 January 1979 and time integrated for 3 years. The distribution of sea surface temperature is prescribed based on monthly averaged climatological data.

Figure 1 (a) shows the 8-year average (1979-1986) zonal mean ozone mixing ratio (μ gm/gm) for January (1979-1986) [Nagatani et al., 1988] from the Nimbus 7 Solar Backscatter Ultra Violet (SBUV) instrument, and Figure 1 (b) is the simulated results from the MRI GCM. The latitudinal direction is opposite in these figures. The maximum value and the height over the equator 16 ppmm is almost coincide with the observation, however the value near the tropopause is systematically larger in the simulation.

Figure 2 shows the same figure as the Figure 1 but the month of July. The MRI GCM result is almost coincide with the observation where the maximum value in the srtatosphere locates in the summer hemisphere.

Figure 3 indicates the seasonal change of ozone at the equator from the observation and the simulation. Ozone at the equator decreases in the upper stratosphere and increases in the middle stratosphere from January to July. Figure 4 is the zonal mean ozone difference between the January and July simulations. In the middle stratosphere ozone has large values in summer

when the temperature has high values; in the upper stratosphere the change has opposite sign.

As a result the MRI GCM roughly simulate the seasonal variation of ozone with the simplified ozone photochemical processes. Further study is needed with the coupling process between the ozone photochemical process and the dynamical processes in the course of seasonal march.

Reference

Atmospheric Ozone as a Climate Gas. NATO ASI Series, Vol32, 465pp, 1995 Edited by W.-C.Wang and I.S.A. Isaksen

D.A. Randall, I. Yagai, et.al., :Analysis of snow feedbacks in 14 in general circulation models. J. Geophys. Res., 99, 20757-20771, 1994.

Nagatani, M.N., A.J. Miller, K.W. Johnson and M.E. Gelman: An eight-year climatology of meteorological and SBUV ozone data. NOAA Technical report NWS 40, National Oceanic and Atmospheric Administration, 125 pp, 1988.

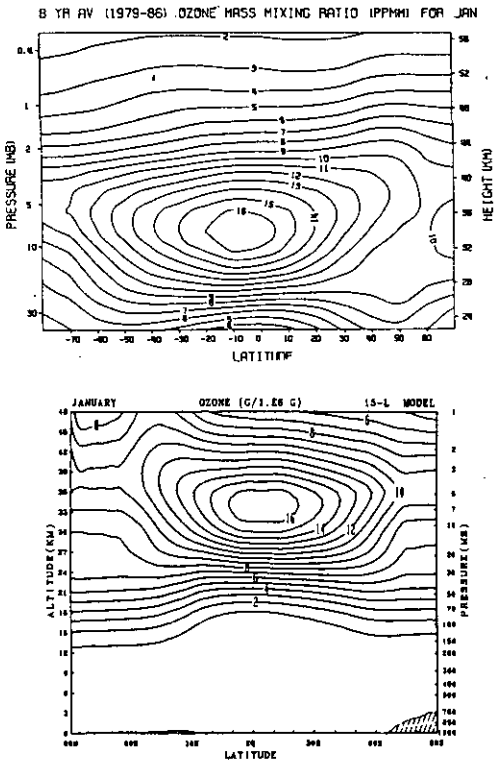

Figure 1: (a)The 8-year average (1979-1986) zonal mean ozone mixing ratio (μ gm/gm) for January (1979-1986) [Nagatani et al., 1988] from the Nimbus 7 Solar Backscatter Ultra Violet (SBUV) instrument and (b) the simulated results from the MRI GCM.

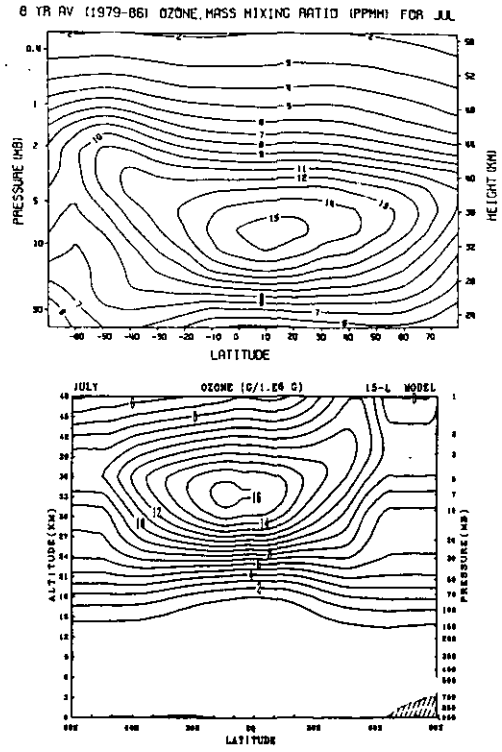

Figure 2: The same as in Figure 1 but for the month of July.

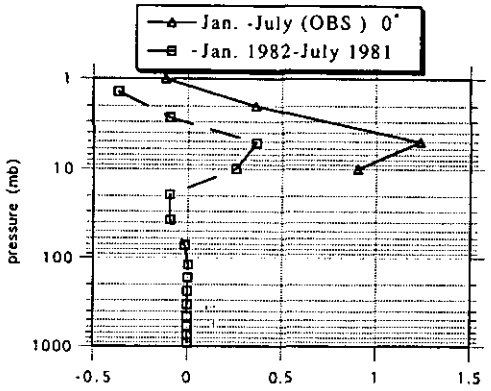

Figure 3: The seasonal change of ozone at the equator from the observation and the simulation (January-July).

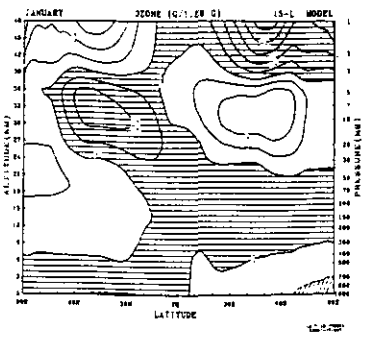

Figure 4: The zonal mean ozone difference between the January and July by the MRI GCM simulations. Negative values are shaded.